Acta Crystallographica Section D
Biological Crystallography
ISSN 0907-4449

Solution and structure of an alternating D,L-peptide

Eftichia Alexopoulos,[a] Andrea Küsel,[b] George M. Sheldrick,[a] Ulf Diederichsen[b] and Isabel Usón[c]*

[a]Lehrstuhl für Strukturchemie, Institut für Anorganische Chemie, Universität Göttingen, Tammannstrasse 4, 37077 Göttingen, Germany, [b]Institut für Organische und Biomolekulare Chemie, Universität Göttingen, Tammannstrasse 2, 37077 Göttingen, Germany, and [c]ICREA at Instituto de Biología Molecular de Barcelona (IBMB-CSIC), Jordi Girona 18-26, 08034 Barcelona, Spain

Correspondence e-mail: uson@ibmb.csic.es

Received 9 June 2004
Accepted 8 September 2004

PDB Reference: H-(L-Tyr-D-Tyr)$_4$-L-Lys-OH, 1uno, r1unosf.

The crystal structure of H-(L-Tyr-D-Tyr)$_4$-L-Lys-OH has been determined to 1.3 Å resolution. The D,L-alternating peptide crystallizes in the tetragonal system, space group $P4_32_12$, with unit-cell parameters $a = b = 27.99$ (3), $c = 78.93$ (8) Å. The crystals contain two molecules in the asymmetric unit that form a double-stranded right-handed antiparallel β-helix. The structure has been solved by SIRAS using a crystal soaked in an iodide-containing solution for 1 min. The programs *SHELXD* and *SHELXE* were used to determine the iodide substructure and also the experimental electron-density map. Using the coordinates of known D,L-peptides deposited in the PDB, several attempts were made to solve the structure by molecular-replacement techniques. Although the backbone of the MR model selected shows great similarity and was used to trace the actual peptide structure in the map, it was not possible to obtain the correct solution before the experimental phases became available. The correct fragment orientations are easily determined, but the same does not apply to the translation search. Nevertheless, insights into fragment search and expansion were gained from the tests described in this paper. The correlation coefficient calculated with the resolution shell of data around 2.4 Å, a distance corresponding to most 1—3 interatomic vectors, is a particularly good discriminator of correct orientations in the rotation search of small fragments.

1. Introduction

The motif of hollow tubular structures that are engineered to self-assemble into ordered nanotubes has been pursued by synthetic organic chemists in recent years (Bong *et al.*, 2001). Of the various compound classes that adopt such structures, peptides with a D,L-alternating configuration of the C^α atoms are an example found in nature. The classical example is the natural monovalent ion-channel pentadecapeptide antibiotic gramicidin A, which forms a double-stranded antiparallel β-helical dimer (Langs, 1989). This helical dimer encircles a cavity, resulting in a membrane-spanning channel. Structurally, the D,L-alternating peptides are of interest because of their flexibility. In the case of gramicidin A, it has been shown that under different conditions (ion concentration and pH of the environment) not only the number of residues per turn and the pitch, and therefore the channel diameter, but also the handedness of the helix varies (Burkhart *et al.*, 1998). The structures of linear D,L-alternating peptides of sufficient length (octapeptides or longer) that have been determined to date show the gramicidin β-helix structure, such as Boc-(L-Val-D-Val)$_4$-OMe, Boc-(L-Phe-D-Phe)$_4$-OMe (Di Blasio *et al.*, 1989*a*,*b*). This is also the case for the N-methylated and therefore conformationally constrained H-(L-Nle-D-Nle)$_4$-OH (Fenude *et al.*, 1989).

A single-stranded helix structure in chloroform solution has been interpreted from NMR data but has not so far been confirmed in crystals (Lorenzi *et al.*, 1982). However, one shorter D,L-alternating hexapeptide *tert*-butyloxycarbonyl-(D-alloisoleucyl-L-isoleucyl)$_3$ methyl ester monohydrate adopts a type II β-turn structure rather than a double-stranded helix, possibly owing to the protecting groups at the N- and C-terminal ends (Di Blasio *et al.*, 1995).

Cyclic peptides (D-aa-L-aa)$_n$ (n = 2, 4, 6 or 8; aa = valine, leucine or phenylalanine and others) have been characterized by various structural techniques. The dipeptides are strongly constrained by the nearly planar six-membered ring formed by the peptide backbone, with the carbonyl O atoms in the plane and the side chains oriented perpendicular to the plane (Benedetti, 1982). The larger rings proved to be remarkably insoluble compared with their linear analogues. This behaviour suggested the formation of tubular parallel or antiparallel cylindrical β-sheet-like structures by the association of β-rings that had been observed in the crystal structures of the cyclo-(D-Val-L-Val)$_3$ and cyclo-(D-Phe-L-Phe)$_3$ surrounded by solvent (Pavone *et al.*, 1989). Antiparallel dimers were designed by the use of cyclic peptides with half of the peptides N-methylated and therefore only one surface capable of stacking interactions (Sun & Lorenzi, 1994). More recently, macromolecular nanotubes generated by the self-assembly of cyclic D,L-alternating peptides have been characterized by electron microscopy, electron diffraction and FT-IR with the aid of crystal structure modelling (Hartgerink *et al.*, 1998). An interesting aspect of such assemblies is their biological activity as antibacterial agents which is derived from increased membrane permeability and has been tested *in vitro* against a wide variety of Gram-positive and Gram-negative pathogens (Fernández-López *et al.*, 2001).

The tight and effective hydrogen-bonding interactions between the backbone carbonyl and amide groups arising in the formation of the double-stranded β-helix involves practically all hydrogen-bond donors and acceptors in intermolecular contacts. This is also the case in the formation of the cylindrical parallel or antiparallel β-sheets invoked in nanotubes. Both situations represent efficiently stabilized structures and determine the orientation of the side chains to the exterior of the tubes formed by the backbone atoms. Thus, in the gramicidin helix all side chains are oriented towards the membrane and in cyclic peptides they are oriented outwards within the plane of the cyclic peptide. In an extended peptide adopting a β-sheet-like secondary structure analogous to a longitudinally sliced nanotube, all side chains would be oriented in the same direction on one side of the strand (Diederichsen, 1997).

As the structures determined for linear D,L-alternating peptides have been shown to be highly sensitive to the medium, it was of interest to grow crystals of D,L-alternating peptides from water rather than organic solvents. In case of the oligomer H-(L-Tyr-D-Tyr)$_4$-L-Lys-OH, destacking of the side-chain chromophores was observed in water by a sigmoidal increase of the UV absorption with rising temperature. Using this well established method for the determination of DNA double-strand dissociation (Saenger, 1988), a rather surprising stability of T_m = 312 K in aqueous phosphate buffer (pH 7, 0.01 *M* Na_2HPO_4/H_3PO_4, 0.1 *M* NaCl) was derived for the tyrosine oligomer (Fig. 1). The nature of the aromatic–aromatic interactions and the question whether water as a solvent cage propagates the aggregation of the aromatic side chains was a major motivation for the structural investigation. Firstly, the phenyl oligomer H-(L-Phe-D-Phe)$_4$-OH was synthesized, but it turned out to be insoluble in water. Since even H-(L-Phe-D-Phe)$_4$-L-Lys-OH, which has a cationic side chain at the C-terminus, had not provided sufficient solubility for structural studies in polar solvents, the corresponding tyrosine peptide was investigated. The crystallization of peptide H-(L-Tyr-D-Tyr)$_4$-L-Lys-OH from water and its structure elucidation are reported. The helical dimers found are especially interesting because of their terminal stacking in rods and the water-mediated interaction between these rods; these peptides are strong candidates for membrane-channel formation.

2. Materials and methods

2.1. Crystallization

The D,L-peptide was synthesized by the Fmoc solid-phase method (Chan & White, 2000) and purified *via* HPLC. Native crystals were grown by vapour diffusion at 277 K in 4 µl hanging drops from a peptide solution with a concentration of 10 mg ml^{-1} using 30% MPD, 0.02 *M* sodium bromide and 0.5 *M* ammonium sulfate in 100 m*M* HEPES buffer pH 7.5 as a precipitant in a 1:1 ratio. Single crystals grew over a period of one week. Crystals to be used for iodide soaking were grown under the same conditions but in the absence of sodium bromide. These crystals were soaked for 1 min in precipitant solution containing 1 *M* lithium iodide. In both cases, no cryoprotectant was required because the crystallization solution had a glass-like freezing behaviour. Both the native and the soaked crystals belong to the tetragonal space group $P4_32_12$, with unit-cell parameters $a = b = 27.99\,(3)$, $c = 78.93\,(8)$ Å, $V = 61\,878.27$ Å^3. The asymmetric unit contains two peptide molecules and 40% solvent.

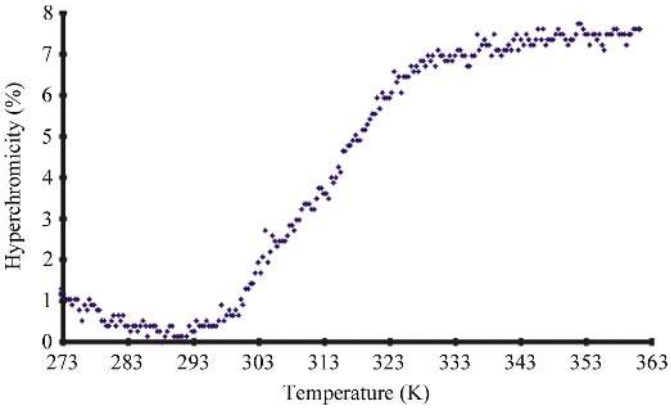

Figure 1
Temperature-dependent increase in UV absorption (hyperchromicity) for the oligomer H-(L-Tyr-D-Tyr)$_4$-L-Lys-OH measured at 230 nm in aqueous phosphate buffer (pH 7, 0.01 *M* Na_2HPO_4/H_3PO_4, 0.1 *M* NaCl).

Table 1
Statistics of X-ray data collection.

Values in parentheses are for the outer resolution shell (0.1 Å).

Data set	Native, in-house	Native, Hamburg	Native, merged	I^--soak, in-house	I^--soak, Hamburg	I^--soak, merged
Resolution (Å)	2.20	1.30	1.30	2.45	2.49	2.45
R_{sym}† (%)	5.51	7.10	8.88	13.66	8.48	10.64
Completeness (%)	96.7 (80.7)	98.7 (96.9)	99.0 (96.9)	77.5 (20.6)	99.8 (98.9)	94.0 (58.3)
$I/\sigma(I)$	10.33 (7.54)	3.95 (1.50)	14.35 (1.50)	6.30 (5.14)	6.92 (6.71)	27.08 (8.05)
Redundancy	11.6 (3.51)	8.00 (6.22)	—	4.71 (0.41)	8.02 (7.36)	—

† $R_{sym} = \sum |I_{hkl} - \langle I_{hkl}\rangle| / \sum |I_{hkl}|$.

2.2. X-ray data collection

Two low-temperature native data sets were collected. The first data set was recorded in-house to 2.2 Å resolution on a Bruker SMART 6000 CCD detector coupled to a Cu rotating-anode generator (Cu $K\alpha$, λ = 1.5418 Å) and an Oxford Cryostream cooling device at a temperature of 100 K. A thin-slicing mode was used with an oscillation angle of 0.2°, a crystal-to-detector distance of 55 mm and an exposure time of 60 s. A total of 22 183 unique data were measured from a crystal of dimensions 0.2 × 0.2 × 0.1 mm mounted in a loop. Data integration and scaling was performed using the programs *PROTEUM* and *SADABS* (Bruker AXS). The crystal was returned to the storage dewar and a second data set was subsequently collected at EMBL, c/o DESY, Hamburg on the X13 synchrotron beamline with an X-ray wavelength of 0.8015 Å using a MAR CCD detector. A high-resolution data set from 15 to 1.3 Å with an oscillation angle of 0.5° and a low-resolution data set to 2.45 Å with an oscillation angle of 0.5° were measured. Owing to fluctuations in the detector temperature, two separate high-resolution data sets had to be integrated with *DENZO* (Otwinowski & Minor, 1997) but could be merged together with the low-resolution data during scaling with *SCALEPACK* (Otwinowski & Minor, 1997). This marred the quality of the synchrotron data in comparison to the in-house data recorded on the same crystal in spite of the improved resolution.

For the iodide-soaked crystal, a first data set was measured in-house on a MAR345 image plate with a Bruker rotating Cu anode generator and an Osmic mirror system (Cu $K\alpha$, λ = 1.5418 Å) to a resolution of 2.45 Å at a temperature of 100 K. The data set was originally intended as a test for the quality of the crystal, but was nevertheless used for the structure solution, in spite of its rather low completeness (77.5%). The data processing was performed with *DENZO* and *SCALEPACK*. The frozen crystal was transported to EMBL, c/o DESY, Hamburg and data were collected on synchrotron beamline BW7A at 100 K with an X-ray wavelength of 0.954 Å using a MAR165 CCD detector. Surprisingly, the resolution attained was slightly lower than that attained in-house (25–2.49 Å), which could be a result of crystal damage upon transfer from the diffractometer to the transport dewar and from this to the beamline. These data were processed with *HKL*2000. Reflection data statistics for all data sets are shown in Table 1.

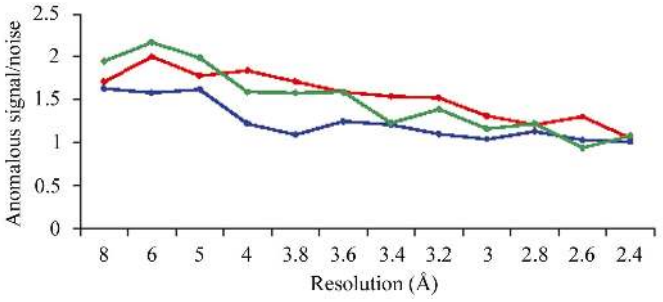

Figure 2
Anomalous signal-to-noise ratio (mean value of $|F_+ - F_-|$ divided by its s.u.) against resolution for the in-house data set (red), the BW7A data set (blue) and the merged data set (green).

2.3. Structure solution

The two native data sets were collected from the same crystal and could be merged into a single data set with 10 560 averaged reflections. R_{merge} is 9% and shows a good fit of the common reflections. As the crystal was grown in a solution containing bromine ions, the data were checked for bromine anomalous signal, but none could be detected. The resolution of 1.3 Å is probably not quite adequate for the *ab initio* solution of a structure consisting entirely of light atoms.

The iodide-derivative data sets were also collected from one crystal and were merged with an R_{merge} of 11%. The merged data set contains 2139 averaged reflections to 2.45 Å resolution. The anomalous signal-to-noise ratio of the data sets is shown in Fig. 2. In general, the iodide anomalous signal is rather weak and becomes insignificant at a resolution higher than 3.8 Å. Thus, it was not possible to solve the structure using the iodide anomalous signal on its own (SAD).

Local scaling of the merged native and the merged derivative data gave an R_{int} of 17%, suggesting that the data sets were sufficiently isomorphous for structure solution by SIRAS. The resolution at which the data are truncated is critical for locating heavy-atom sites from noisy SIRAS data. By excluding high-resolution shells with none or very low anomalous signal the noise and problems caused by lack of isomorphism are reduced. In this case, the data were truncated to 2.5 Å. In a run of 1000 tries and with a minimum E value of 1.3, *SHELXD* (Sheldrick *et al.*, 2001) found six heavy-atom sites, two of which were strongly occupied and two very weakly. 400 cycles of density modification with 40% solvent were performed with *SHELXE* (Sheldrick, 2002) for both enantiomorphs. The mean estimated map CC was calculated for both heavy-atom enantiomorphs; it was highest for $P4_32_12$, identifying it as the correct space group. Two further figures of merit of the map used were the contrast and the connectivity. In the sphere-of-influence algorithm incorporated in *SHELXE* the variance V of density on a spherical surface of

Table 2
Refinement progress.

Action	Peptide atoms	Water	Parameters	Restraints	R_1 [$I > 2\sigma(I)$/all]	R_{free} [$I > 2\sigma(I)$/all]
Model building, 1.3 Å	209	—	843	903	0.3145/0.3432	0.3590/0.3810
Water addition, 1.3 Å	209	16	907	903	0.2664/0.2943	0.2920/0.3130
Model completion, 1.3 Å	211	16	915	908	0.2528/0.2799	0.2787/0.2985
Resolution cutoff, 1.4 Å	211	16	915	908	0.2464/0.2650	0.2783/0.2930
Anisotropic scaling, 1.3 Å	211	16	927	908	0.2021/0.2265	0.2314/0.2483
Anisotropic refinement, 1.3 Å	211	16	1975	2570	0.1836/0.2059	0.2346/0.2479
Water addition, 1.3 Å	211	19	939	907	0.1971/0.2216	0.2332/0.2493
Hydrogen addition, 1.3 Å	364	19	1977	2574	0.2042/0.2285	0.2372/0.2537
Final	211	19	939	1	0.1989/0.2230	—

Table 3
Crystal data and refinement statistics.

Unit-cell parameters (Å)	$a = b = 27.99$ (3), $c = 78.93$ (8)
Space group	$P4_32_12$
No. unique reflections	8289 (7883 without R_{free})
Resolution range	20–1.3
R factor ($I > 4\sigma$)	0.1971
R_{free} ($I > 4\sigma$)	0.2332
No. water molecules	19
Data/restraints/parameters	7883/907/939
R.m.s. deviations from idealized geometry	
Bond lengths (Å)	0.011
1,3-Distances (Å)	0.028
Zero chiral volumes (Å^3)	0.072
Non-zero chiral volumes (Å^3)	0.100
Distances from restraint planes (Å)	0.179
Mean B factor (Å^2)	
Main-chain atoms	10.31
Side-chain atoms	18.06
Solvent atoms	24.38

radius 2.42 Å is calculated for each pixel in the map and the pixels with the highest variances (V) are considered to be more likely to be atom positions. In this way some chemical information is added as 2.42 Å is the typical 1,3-distance in proteins and DNA. The variance of V over all pixels is defined as the contrast. The connectivity is the fractions of adjacent pixels that are both either in the solvent or both in protein regions. For this structure both figures showed significant differences starting from the two heavy-atom enantiomorphs, being distinctly lower for $P4_12_12$ (contrast = 0.373, connectivity = 0.877) than for $P4_32_12$ (contrast = 0.551, connectivity = 0.902). Finally, a pseudo-free correlation coefficient is calculated, leaving out 10% of reflections at random and performing one cycle of density modification ($P4_32_12$, 84.89%; $P4_12_12$, 69.15%). The electron-density map obtained could be traced by hand using the structure of a known D,L-alternating peptide [*t*-Boc-(L-Phe-D-Phe)$_4$-OMe] (Lorenzi *et al.*, 1982) as a guide.

2.4. Structure refinement

The model was subject to least-squares refinement with *SHELXL*97 (Sheldrick & Schneider, 1997) against F^2 of the synchrotron data using a conjugate-gradient algorithm. A set of reflections representing 5% of the overall reflections was chosen in thin shells, in case non-crystallographic symmetry should be applied, to define an R_{free} set for cross-validation (Brünger, 1992). The refinement stages are summarized in Table 2. In the first cycle the double helix was built by tracing the map and using the D,L-alternating peptide *t*-Boc-(L-Phe-D-Phe)$_4$-OMe as a template. Geometric restraints for 1,2- and 1,3-distances were defined using the Engh & Huber (1991) values as targets. Planarity, anti-bumping and chiral volume restraints were also included. The diffuse solvent region was accounted for by a two-parameter model based on Babinet's principle (Moews & Kretsinger, 1975*a*,*b*). The initial R_{work} was 0.31 (R_{free} = 0.36). As a next step, water molecules were added manually from the map, selecting from the highest electron-density peaks those making reasonable contacts. The approximately spherical shape of the $F_o - F_c$ electron density corresponding to water molecules was confirmed in the σ-weighted map. Completion of the model gave an R_{work} of 0.25 and an R_{free} of 0.28. Truncation of the data to a resolution of 1.4 Å improved the R_{work}, but did not affect the R_{free} significantly and was therefore not applied.

Taking into account the detector-temperature fluctuations and the long needle-like shape of the crystals, an anisotropic scaling correction was considered. In this procedure, 12 anisotropic scaling parameters are refined for the otherwise isotropic structure (Usón *et al.*, 1999). Nevertheless, an anisotropic refinement of the atomic B values, which is recommended at this resolution, led to better results for R_{work} than the scaling correction (see Table 2). One should bear in mind though that anisotropic scaling involves only 12 extra parameters, leading to a data-to-parameter ratio of 8.5:1, whereas the ratio in the case of the anisotropic refinement is 4:1. This is also reflected by the minimal improvement of the R_{free} values (less than 0.5%), indicating that the effect on the R_{work} is purely cosmetic and that anisotropic scaling should be favoured rather than the anisotropic refinement of individual B factors.

The inclusion of H atoms at geometrically calculated positions and their refinement using a riding model did not lead to any improvement, but increased the R values. As a further step, the structure was refined to convergence with 19 water molecules to the final values R_{work} = 0.20 and R_{free} = 0.23. Finally, full-matrix least-squares refinement was performed against all data (including the R_{free} set) to calculate standard uncertainties (the s.u. table has been provided as supplementary material[1]). The refinement proved to be unstable, so the parameters had to be kept at fixed values to prevent excessive shifts. Further details of the refinement statistics are presented in Table 3.

[1] Supplementary material has been deposited in the IUCr electronic archive (Reference: DZ5022). Details for accessing these data are given at the back of the journal.

Table 4
Conformational parameters of H-(L-Tyr-D-Tyr)$_4$-L-Lys-OH.

Angle	L	D	L	D	L	D	L	D
Strand 1								
φ (N—Cα)		150	−100	150	−111	153	−114	147
ψ (C$^{\alpha}$—C)	119	−86	150	−130	140	−74	143	−111
χ_1 (C$^{\alpha}$—C$^{\beta}$)	175	168	−64	−177	171	158	−60	176
χ_2 (C$^{\beta}$—C$^{\gamma}$)	83	104	92	113	71	41	−77	−79
Strand 2								
φ (N—C$^{\alpha}$)		151	−94	136	−106	149	−116	
ψ (C$^{\alpha}$—C)	117	−89	158	−140	146	−72	146	
χ_1 (C$^{\alpha}$—C$^{\beta}$)	−63	165	−68	75	−65	168	−60	
χ_2 (C$^{\beta}$—C$^{\gamma}$)	97	−119	102	−111	−91	−4	105	

3. Results and discussion

3.1. Description of the structure

The asymmetric unit of the tetragonal H-(L-Tyr-D-Tyr)$_4$-L-Lys-OH contains a single dimer and 19 water molecules. Two stereoviews of the dimer are shown in Fig. 3. It is a right-handed double-stranded antiparallel $\beta^{5.6}$ helix with an overall length of 19.7 Å. The average inner channel diameter as calculated for the equivalent C$^{\alpha}$ atoms of each strand is ∼6 Å, varying from 4.7 to 7.2 Å. Taking van der Waals radii into account, the dimer has an inner radius of 2.2 Å, a value which would allow the transfer of alkali metal cations through the channel without widening of the helix diameter, but not of water molecules.

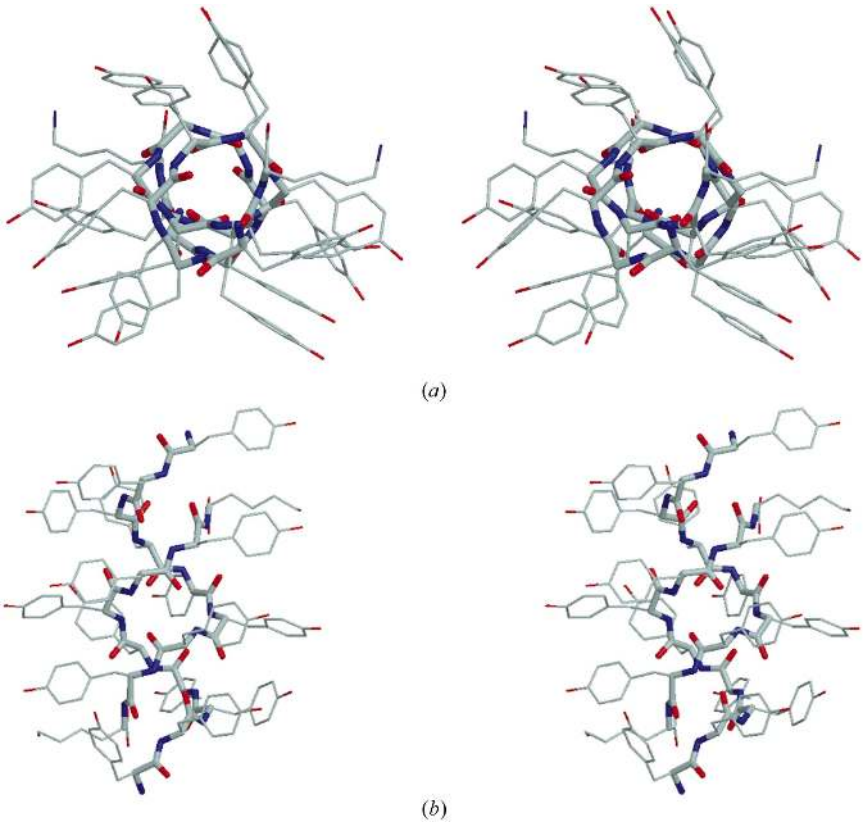

Figure 3
(*a*) Stereo projection of H-(L-Tyr-D-Tyr)$_4$-L-Lys-OH along the double-helix axis; (*b*) stereo projection of the right-handed antiparallel double-stranded β-helix of H-(L-Tyr-D-Tyr)$_4$-L-Lys-OH.

As is typical for alternating D,L-peptides, the association of the two helical chains is stabilized by systematic NH···O=C hydrogen bonds between donor and acceptor groups of different strands. Seven N—H groups of one chain are hydrogen bonded to seven O=C groups of the other and *vice versa* (average N···O distance is 2.9 Å). The two remaining N—H groups of each chain connect the dimer in both directions of the helix with the next symmetry-equivalent dimer. In this way pipes are formed along the crystallographic *z* axis.

These pipes are linked to each other *via* a complicated water network. Three tyrosines of one chain and five of the other are connected with symmetry equivalents or with each other *via* 17 water molecules. The hydrogen bonds are formed by the OH groups of the tyrosines, which either interact *via* the water molecules or directly with the OH groups of symmetry-equivalent residues (Fig. 4).

Owing to this tight water network, the OH groups of the tyrosines cluster in the direction of the contact surface with the next chain (Fig. 5), preventing π-stacking of the aromatic rings. This stacking has nevertheless been observed in the structure of H-(L-Phe-D-Phe)$_4$-OH peptide crystallized from organic solvents (Lorenzi *et al.*, 1982). An overview of the conformational parameters of the helix is shown in Table 4. The average φ/ψ torsion angles are 147.33 ± 1.55/−102.25 ± 1.68° and −119.05 ± 1.72/139.91 ± 1.53° for the D- and L-residues, respectively. The side-chain conformation of the tyrosines is defined primarily by the χ_1 and the χ_2 torsion angles. For χ_1, in one helical chain there are four g^-, three *trans* and one g^+ conformations, whereas in the other the preferred conformation is *trans* (six times) with two g^-. This observation deviates slightly from the average geometric parameters reported in the literature (Benedetti *et al.*, 1983), which show a preference for the g^- conformation, and is probably an effect of the hydrogen bonds to the symmetry-equivalent chains. The distribution of the χ_2 torsion angles can be expressed in the range 0–180°, because variation of χ_2 has almost twofold symmetry in the tyrosine residue. With the exception of one D-tyrosine residue, the values are in the expected range 70–120°.

All of the previous alternating non-cyclic D,L-peptide structures show the double-stranded antiparallel β-helix motif, but were crystallized from organic solvents. A comparison of the structure with them is therefore difficult. Many of the structural details of the H-(L-Tyr-D-Tyr)$_4$-L-Lys-OH, such as the crystal packing, can be explained by the connecting water network, which is not present in the other structures. Nevertheless, in all cases the amino-acid side chains are on the same side of the β-helix, oriented towards the solvent. In that way, an

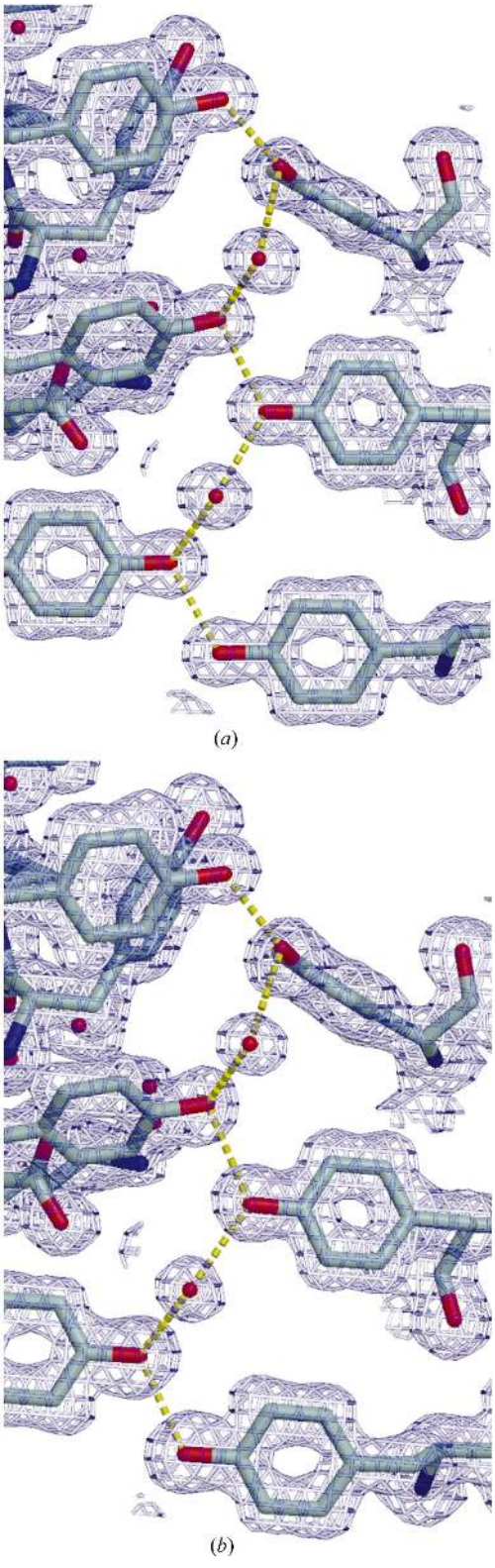

Figure 4
(*a*) View of the electron density of part of the water network between two symmetry-related molecules. The hydrogen bonds are shown as yellow dashed lines; water O atoms are red. The σ_A-weighted map was obtained after the final refinement of the structure with *SHELXL*. (*b*) View of the electron density of part of the water network between two symmetry-related molecules as seen in the first experimental map obtained with *SHELXE*. Again, hydrogen bonds are shown as yellow dashed lines, while water O atoms are red.

inner channel is formed, which is in most cases large enough to allow the transfer of ions. The most typical example of such a structure is the pentadecapeptide antibiotic gramicidin A. Gramicidin A is a naturally occurring product of *Bacillus brevis* known to form ion channels in synthetic and natural membranes. It seems to be selective for monovalent cations such as H_3O^+, Tl^+, NH_4^+ and the alkali metals. Several crystal structures of gramicidin have been reported, either complexed with cations or in an uncomplexed form. The number of amino acids per turn differs from structure to structure, defining various sizes for the channel that could accommodate various unsolvated ions, from K^+ to Cs^+, and showing a certain flexibility of the helix. Theoretically, it could be possible for the H-(L-Tyr-D-Tyr)$_4$-L-Lys-OH to form ionic conductors.

3.2. Structure-solution attempts by molecular replacement or fragment search and expansion with density modification

The effective resolution of the data set of 1.3 Å, but with modest quality at high resolution as a result of the detector instability, appears to put the problem beyond the range of direct methods as currently implemented.

On the other hand, the previously known structures of both gramicidin A and poly-D,L-Phe afford suitable models either for molecular replacement at low resolution or for searching for smaller but more precise fragments at high resolution.

Molecular replacement was extensively tried using a poly-D,L-Ala double helix (78 of the total 212 peptide atoms) but no correct solution could be obtained using classical methods, either with *COMO* (Jogl *et al.*, 2001) performing a limited six-dimensional search around the rotation-function maxima or with *EPMR* (Kissinger *et al.*, 1999) in a stochastic six-dimensional search. Indeed, for any resolution limits, the figures of merit characterizing the correct position are worse than those corresponding to some of the misplaced fragments. Interestingly, the rotation function leads to a more or less accurate but basically correct orientation of the fragment, but the translation search fails. One possible snag lies in the pronounced anisotropy of the data. Still, once the structure was known, MR attempts using data that had been anisotropically scaled again failed to lead to structure solution.

The correctly oriented search model can be placed by hand in the SIRAS 3 Å experimental map. Density modification with the program *SHELXE* (Sheldrick, 2002), starting with phases calculated from the fragments, then leads to a correctly phased map using the merged data to a resolution of 1.7 Å or better. In fact, at the highest resolution (1.3 Å) phasing works starting from as few as ten accurately positioned starting atoms (D-Ala-L-Ala fragment). For comparison, peak-list optimization (Sheldrick & Gould, 1995) at 1.3 Å starting with the 78 atoms of the poly-D,L-Ala fragment does not lead to structure determination.

As the translation function failed, solution of the structure in *P*1, where the correct rotation function may position 1/8 of the contents in the asymmetric unit, was attempted instead. After expanding the data from $P4_32_12$ to *P*1, a promising strategy to determine the correct orientation of a small frag-

ment at high resolution is a rotation search to find local maxima using data in a given resolution shell and cross-validation (Fujinaga & Read, 1987) of the resulting orientation with data from a different resolution shell. Table 5 summarizes the figures of merit obtained in the various tests along with a scoring of their usefulness in identifying correct orientations. Fig. 6 shows six plots with the projection of rotation solutions of different strategies, showing results using the more regularly helical search fragment made up of 78 atoms and the corresponding piece of the final refined structure which describes a more irregular helix. At low resolution (Figs. 6*a* and 6*b*) most search attempts end with roughly well oriented fragments and they can be discriminated from fundamentally wrong orientations through both figures of merit. Nevertheless, such roughly correct solutions are not well discriminated among themselves, so that solutions with the best figures of merit still show large deviations from the optimal position and score poorly if higher resolution data are used for cross-validation. At medium resolution (Figs. 6*c* and 6*d*), between 3 and 1.8 Å, using the strongest data for the search and all data for cross-validation, the search leads in most trials to an incorrectly placed fragment, a very flat distribution of the figures of merit and only in the case of the perfect fragment to a correct discrimination related to figures of merit. In the case of the model fragment the conclusion derived from the figures of merit is inevitably wrong. On the contrary, if data from the resolution shell between 2.45 and 2.0 Å (Fig. 6*f*) are used for cross-validation in the case of the ideal fragment, a larger spread of values is observed and the cross-validation figure of merit discriminates fragments that are optimally placed from roughly well placed or completely wrong ones. This resolution shell contains the values of most 1—3 bonded interatomic distances in a macromolecule and their projections perpendicular to the diffraction planes. This is reflected in the local maximum shown in the distribution of average squared normalized structure-factor amplitudes as a function of resolution in this region (Morris & Bricogne, 2003). This explains its effectiveness in characterizing the orientation of a fragment of the structure. Interestingly, also in the case of the model search fragment (Fig. 6*e*), using all data in the resolution shell 2.45–2.3 Å to calculate the cross-validation figure of merit is the best strategy. In this case, using data beyond 2.2 Å for cross-validation rather impairs the identification of correct orientations. The discrimination is less perfect than for an ideal model, as also incorrectly placed fragments may show high values, but besides such spurious values the correct solutions show a high degree of accuracy. The presence of spurious solutions points out the convenience of using fragment rotation search at high resolution in a multisolution frame to generate promising starting rotations that have to be tried in turn. Using data in the resolution shell 2.8–2.6 Å for cross-validation for comparison purposes proved to be utterly ineffective and the same can be said of higher resolution shells, although smaller more accurate fragments might allow exploitation of the higher resolution. Relying only on the resolution shell 2.45–2.35 Å for the rotation search was not effective either. It would be interesting to check the effect of data in the resolution shell 1.2–1.1 Å, which according to Morris & Bricogne contains the most stereochemical information, but the resolution of the data do not extend this far. In the case of the structure of a cycloamylose composed of 26 glucose units (Gessler *et al.*, 1999), solved generating starting sets of atoms for *SHELXD* from an oriented diglucose fragment, the resolution shell 1.5–1.2 Å was used for the search and between 1.2 and 1.1 Å for cross-validation.

A way around finding the correct translation for the fragment, as in the classical molecular-replacement frame, would be to attempt expansion of the structure starting with a correctly oriented fragment in *P*1. Fig. 7(*a*) shows the orientation determined for the search fragment superimposed on

Table 5
Cross-validation CC dependence on resolution and its reliability for discrimination.

	Perfect fragment			Real search fragment		
Resolution shell (Å)	Max. CC	Average CC	Cross-validation discrimination	Max. CC	Average CC	Cross-validation discrimination
For search						
3–1.8	7.12	3.93		5.28	4.00	
For cross-validation						
2.45–1.85	8.39	3.90	Perfect	5.41	3.92	Fails
2.45–2.0	10.26	4.08	Perfect	5.81	3.02	Weak
2.45–2.1	12.05	4.14	Perfect	7.36	3.30	Weak
2.45–2.2	13.91	4.42	Perfect	9.78	2.71	Fair
2.45–2.3	13.10	3.49	Perfect	10.66	2.33	Fair
2.4–2.3	18.03	4.04	Perfect	12.08	2.79	Fair
2.45–2.35	11.57	3.51	Perfect	12.44	2.27	Fair
2.8–2.6	12.16	3.31	Fails	12.69	4.43	Fails

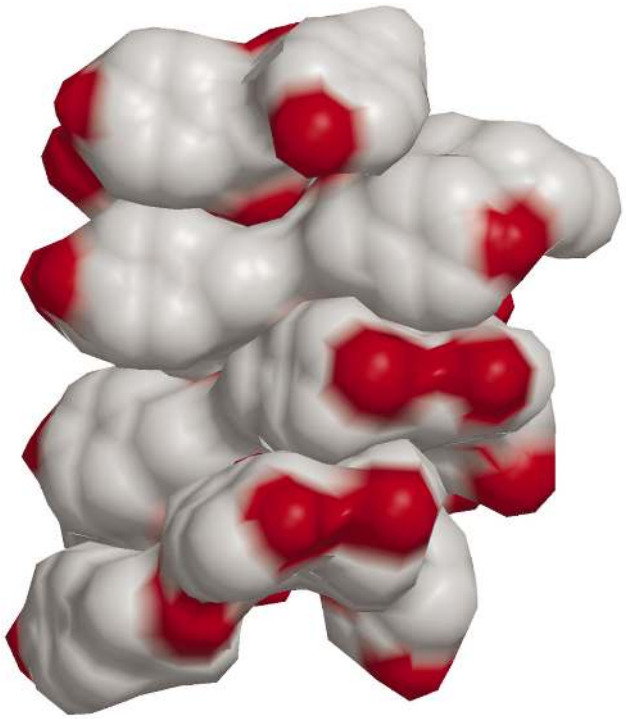

Figure 5
Surface of the helix of H-(L-Tyr-D-Tyr)$_4$-L-Lys-OH, as calculated with *MSMS* (Sanner *et al.*, 1996). O atoms are shown in red.

the crystal packing. The expansion of the structure in *P*1 starting from the poly-D,L-Ala double-helix fragment from poly-D,L-Phe does not lead to correct phases (Fig. 7*b*), but the solvent boundaries derived might be sufficient to allow location of the origin in the higher symmetry space group, thus leading to the determination of the correct translation for the oriented search fragment. Exploration of a fragment search for small fragments at high resolution through more sophisticated approaches leading to correct orientation and translation is in progress.

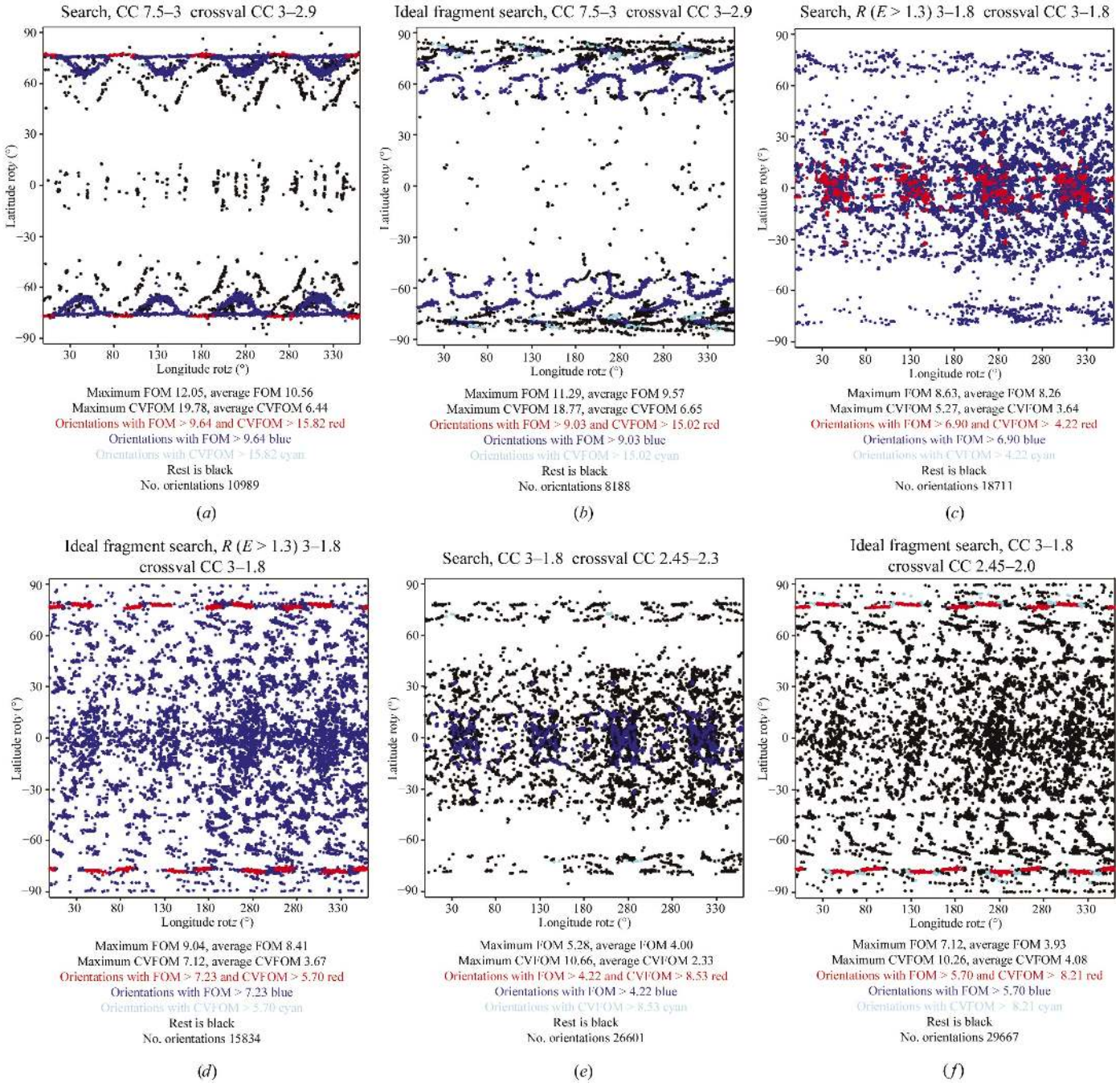

Figure 6
Plane projection of the solutions of the rotation function. The helices form tubes along the crystallographic *z* direction. The model search fragment and the backbone of the molecule (perfect search fragment) have been superimposed optimally and preoriented along the crystallographic *x* axis. The plots express the rotation around the crystallographic *y* axis as latitude and around the crystallographic *z* axis as longitude. The solutions are colour-coded with respect to their figures of merit to indicate they are within 80% of the maximum. FOM is the search figure of merit and CVFOM the cross-validation figure of merit. They are either CC or *R* factor using *E* values stronger than the quoted limit. (*a*) Real search fragment at low resolution, 7.5–2.9 Å. (*b*) Equivalent to (*a*) for perfect fragment. (*c*) Real search fragment at medium resolution, 3–1.8 Å. (*d*) Equivalent to (*c*) for perfect fragment. (*e*) Real search fragment using data in the resolution shell 2.45–2.35 Å for cross-validation. (*f*) Perfect fragment search using data in the resolution shell 2.45–2.35 Å for cross-validation figure of merit shows the best discrimination of solutions.

4. Conclusion

SIRAS techniques were used to solve the structure of a D,L-alternating peptide at high resolution. The molecules form double-stranded double β-helices, a common motif for alternating peptides. Crystals were grown in an aqueous medium and water plays an important role in packing, mediating *via* hydrogen bonds between the helices.

With regard to the rotation search and strategies for the location of the model fragment, it is especially interesting to note that the resolution shell of data around 2.4 Å, a distance corresponding to most 1—3 interatomic vectors, is a particularly good discriminator to identify correctly oriented fragments, not only for a perfect search fragment but even for the real case of an inaccurate fragment.

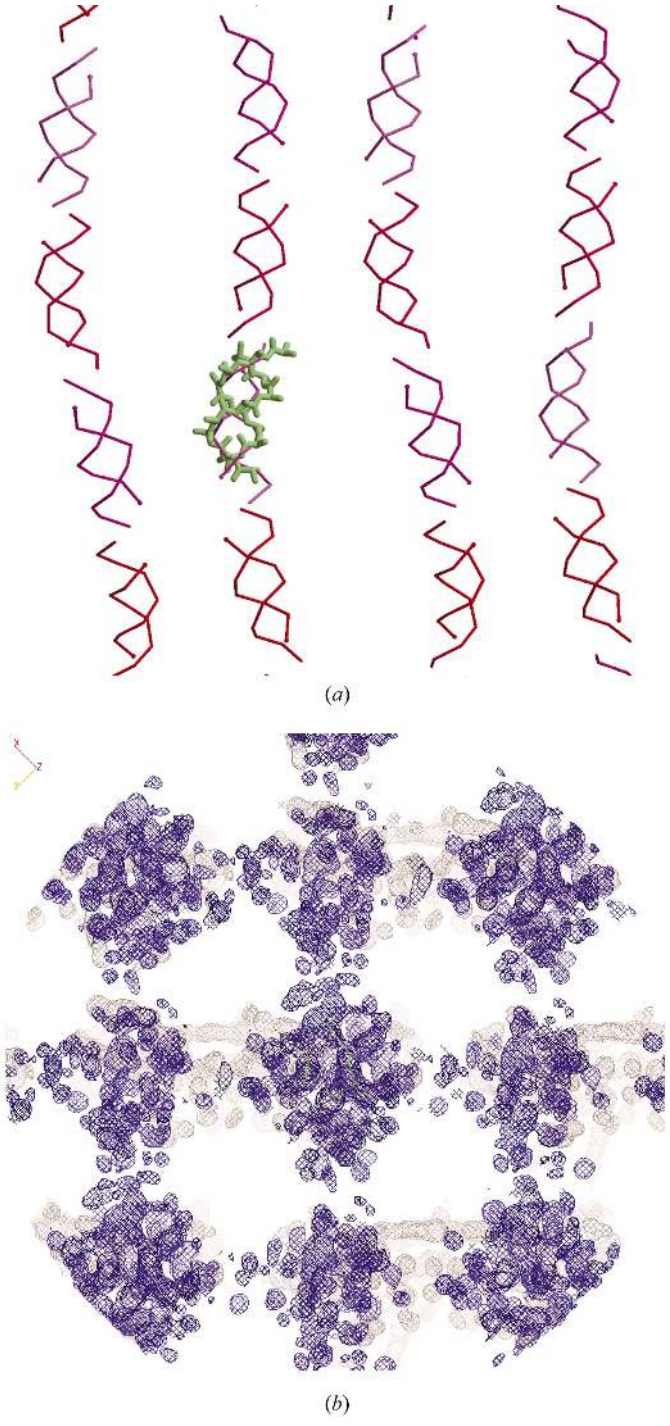

Figure 7
(*a*) The orientation determined for the search fragment shown superimposed on the crystal packing. (*b*) SIRAS map after density modification with *SHELXE* (pink). The mean phase error compared with the final refined model is 13°. The map derived by density modification with *SHELXE* in *P*1 from the correctly oriented fragment is shown in blue. It is not interpretable, but the solvent boundaries could be sufficient to find the origin and the translation in $P4_32_12$.

Data collection at the synchrotron beamlines BW7A and X13 in Hamburg at the EMBL Outstation c/o DESY with assistance from Dr Ehmke Pohl during data collection is gratefully acknowledged. We are thankful to the European Community (Access to Research Infrastructure Action of the Improving Human Potential Programme to the EMBL Hamburg Outstation, contract No. HPRI-1999-CT-00017), to the Fonds der Chemischen Industrie and to the DFG (SFB416) and European Union Integrated Project BIOXHIT for support.

References

Benedetti, E. (1982). *Structure and Conformation of Peptides as Determined by X-ray Crystallography.* In *Chemistry and Biochemistry of Amino Acids, Peptides and Proteins*, Vol. 6, edited by B. Weinstein, pp. 105-184. New York: Marcel Dekker.
Benedetti, E., Morelli, G., Némethy, G. & Scheraga, H. (1983). *Int. J. Pept. Protein Res.* **22**, 1–15.
Bong, D. T., Clark, T. D., Granja, J. R. & Ghadiri, M. R. (2001). *Angew. Chem. Int. Ed.* **40**, 988–1011.
Brünger, A. T. (1992). *Nature (London)*, **355**, 472–475.
Burkhart, B. M., Li, N., Langs, D. A., Pangborn, W. A. & Duax, W. L. (1998). *Proc. Natl Acad. Sci. USA*, **95**, 12950–12955.
Chan, W. C. & White, P. D. (2000). Editors. *Fmoc Solid Phase Peptide Synthesis – A Practical Approach.* Oxford University Press.
Di Blasio, B., Benedetti, E., Pavone, V., Pedone, C., Gerber, C. & Lorenzi, G. P. (1989*a*). *Biopolymers*, **28**, 193–201.
Di Blasio, B., Benedetti, E., Pavone, V., Pedone, C., Gerber, C. & Lorenzi, G. P. (1989*b*). *Biopolymers*, **28**, 203–214.
Di Blasio, B., Del Duca, V., Lombardi, A., Pedone, C., Lorenzi, G. P. & Benedetti, E. (1995). *Int. J. Pept. Protein Res.* **45**, 100–105.
Diederichsen, U. (1997). *Angew. Chem. Int. Ed. Engl.* **36**, 1886–1889.
Engh, R. A. & Huber, R. (1991), *Acta Cryst.* A**47**, 392–400.
Fenude, E., Tomasic, L. & Lorenzi, G. P. (1989). *Biopolymers*, **28**, 185–192.
Fernández-López, S., Kim, H.-S., Choi, E. C., Delgado, M., Granja, J. R., Khasanov, A., Kraehenbuehl, K., Long, G., Weinberger, D. A., Wilcoxen, K. M. & Ghadiri, R. (2001). *Nature (London)*, **412**, 452–455.
Fujinaga, M. & Read, R. J. (1987). *J. Appl. Cryst.* **20**, 517–521.
Gessler, K., Usón, I., Takaha, T., Krauss, N., Smith, S. M., Okada, S., Sheldrick, G. M. & Saenger, W. (1999). *Proc. Natl Acad. Sci. USA*, **96**, 4246–4251.
Hartgerink, J. D., Clark, T. D. & Ghadiri, M. R. (1998). *Chem. Eur. J.* **4**, 1367–1372.
Jogl, G., Tao, X., Xu, Y. & Tong, L. (2001). *Acta Cryst.* D**57**, 1127–1134.
Kissinger, C. R., Gehlhaar, D. K. & Fogel, D. B. (1999). *Acta Cryst.* D**55**, 484–491.
Langs, D. A. (1989). *Biopolymers*, **28**, 259–266.

Lorenzi, G. P., Jäckle, H., Tomasic, L., Rizzo, V. & Pedone, C. (1982). *J. Am. Chem. Soc.* **104**, 1728–1733.
Moews, P. C. & Kretsinger, R. H. (1975*a*). *J. Mol. Biol.* **91**, 201–225.
Moews, P. C. & Kretsinger, R. H. (1975*b*). *J. Mol. Biol.* **91**, 229–232.
Morris, R. J. & Bricogne, G. (2003). *Acta Cryst.* D**59**, 615–617.
Otwinowski, Z. & Minor, W. (1997). *Methods Enzymol.* **276**, 307–326.
Pavone, V., Benedetti, E., Di Blasio, B., Lombardi, A., Pedone, C., Tomasich, L. & Lorenzi, G. P. (1989). *Biopolymers*, **28**, 215–223.
Sanner, M. F., Olson, A. J. & Spehner, J.-C. (1996). *Biopolymers*, **38**, 271–282.
Saenger, W. (1988). *Principles of Nucleic Acid Structure.* New York: Springer-Verlag.
Sheldrick, G. M. (2002). *Z. Kristallogr.* **217**, 644–650.
Sheldrick, G. M. & Gould, R. O. (1995). *Acta Cryst.* B**51**, 423–431.
Sheldrick, G. M., Hauptman, H. A., Weeks, C. M., Miller, R. & Usón, I. (2001). *International Tables for Macromolecular Crystallography*, Vol. *F*, edited by M. G. Rossmann & E. Arnold, ch. 16, pp. 333–345. Dordrecht: Kluwer Academic Publishers.
Sheldrick, G. M. & Schneider, T. R. (1997). *Methods Enzymol.* **277**, 319–343.
Sun, X. & Lorenzi, G. P. (1994). *Helv. Chim. Acta*, **77**, 1520–1526.
Usón, I., Pohl, E., Schneider, T. R., Dauter, Z., Schmidt, A., Fritz, H.-J. & Sheldrick, G. M. (1999). *Acta Cryst.* D**55**, 1158–1167.